BIOCHEMISTRY
including biophysical chemistry & molecular biology
Article

Biochemistry **2010,** *49,* 5859–5869 5859
DOI: 10.1021/bi1004987

Mutagenesis of *Klebsiella aerogenes* UreG To Probe Nickel Binding and Interactions with Other Urease-Related Proteins[†]

Jodi L. Boer,[‡] Soledad Quiroz-Valenzuela,[‡,§] Kimberly L. Anderson,[∥] and Robert P. Hausinger*[,‡,∥]

[‡]*Department of Biochemistry and Molecular Biology, and* [∥]*Department of Microbiology and Molecular Genetics, Michigan State University, East Lansing, Michigan 48824* [§]*Present address: Escuela de Biotecnología, Universidad Santo Tomás, Chile*

Received April 2, 2010; Revised Manuscript Received June 8, 2010

ABSTRACT: UreG is a GTPase required for assembly of the nickel-containing active site of urease. Herein, a *Strep*-tagged *Klebsiella aerogenes* UreG ($UreG_{Str}$) and selected site-directed variants of $UreG_{Str}$ were constructed for studying the *in vivo* effects on urease activation in recombinant *Escherichia coli* cells, characterizing properties of the purified proteins, and analysis of *in vivo* and *in vitro* protein−protein interactions. Whereas the *Strep* tag had no effect on UreG's ability to activate urease, enzyme activity was essentially abolished in the K20A, D49A, C72A, H74A, D80A, and S111A $UreG_{Str}$ variants, with diminished activity also noted with E25A, C28A, and S115A proteins. Lys20 and Asp49 are likely to function in binding/hydrolysis of GTP and binding of Mg, respectively. $UreG_{Str}$ binds one nickel or zinc ion per monomer (K_d ~5 μM for each metal ion) at a binding site that includes Cys72, as shown by a 12-fold increased K_d for nickel ions using C72A $UreG_{Str}$ and by a thiolate-to-nickel charge-transfer band that is absent in the mutant protein. Based on UreG homology to HypB, a GTPase needed for hydrogenase assembly, along with the mutation results, His74 is likely to be an additional metal ligand. *In vivo* pull-down assays revealed Asp80 as critical for stabilizing $UreG_{Str}$ interaction with the UreABC−UreDF complex. *In vitro* pull-down assays demonstrated UreG binding to UreE, with the interaction enhanced by nickel or zinc ions. The metallochaperone UreE is suggested to transfer its bound nickel to UreG in the UreABC−UreDFG complex, with the metal ion subsequently transferring to UreD and then into the nascent active site of urease in a GTP-dependent process.

Urease, a nickel-containing enzyme found in plants and microorganisms, catalyzes the hydrolysis of urea to form ammonia and carbamate, which spontaneously decomposes to carbon dioxide and ammonia (*1*, *2*). Structures of several ureases (*3*−*6*) reveal dinuclear nickel metallocenters deeply buried in structural subunits that coalesce with 3-fold symmetry. With the possible exception of the *Bacillus subtilis* enzyme (*7*), activation of urease has been shown to require a series of accessory proteins to assemble the active site (*1*, *8*). The best understood urease activation system involves the *ureDABCEFG* genes of the enterobacterium *Klebsiella aerogenes* expressed in *Escherichia coli*. This model urease system begins with the structural subunits (UreA, UreB, and UreC) assembling into the urease apoprotein $(UreABC)_3$ (*9*, *10*), with UreD, UreF, and UreG sequentially associating with the apoprotein to form the $(UreABC−UreD)_3$ (*11*), $(UreABC−UreDF)_3$ (*12*), and $(UreABC−UreDFG)_3$ (*13*) activation complexes (Figure 1). Finally, in a process that requires GTP hydrolysis, CO_2 incorporation as an active site carboxylysine, and the nickel-delivering metallochaperone UreE, the active site assembles, and then the accessory proteins release from the active enzyme (*14*, *15*). As described below, the roles of UreD, UreF, and UreG in urease activation are poorly understood.

Studies of UreD are limited to the *K. aerogenes* system. This protein is insoluble when expressed alone; however, a maltose binding protein (MBP)[1]−UreD fusion is soluble and complements a Δ*ureD* urease cluster (*16*). Significantly, the UreD portion of MBP−UreD binds nickel (~2.5 Ni per protomer, K_d ~50 μM), and this protein, when in the UreABC−UreDFG complex, is proposed to transfer the metal ion into the nascent urease active site.

K. aerogenes UreF, like UreD, is insoluble when synthesized separately from the other urease components; however, UreE−UreF and MBP−UreF fusion proteins are soluble and partially characterized (*17*, *18*). In addition, two crystal structures of UreF from *Helicobacter pylori* (PDB codes 3cxn and 2wgl) were solved (unpublished experiments). Computational studies of *Bacillus pasteurii* UreF led to a proposal that the protein functions as a GTPase activating protein (*19*), but no direct evidence for such a role has been reported in any system.

Purified recombinant UreG proteins (subunit M_r 22000−23000) of *K. aerogenes*, *B. pasteurii*, *Mycobacterium tuberculosis*, and *H. pylori* are soluble and contain motifs found in GTPases, although their GTPase activities are very low or nondetectable (*13*, *20*−*22*). Mutation of Lys20 or Thr21 in the GXGKT P-loop motif (a GTPase motif) of the *K. aerogenes* protein abolishes its ability to activate urease (*13*). This region also is critical for *in vitro* activation of the $(UreABC−UreDFG)_3$ complex (*14*). *K. aerogenes* UreG is reported to be monomeric (*13*). In contrast, UreG from *B. pasteurii* and *M. tuberculosis* are dimeric,

[†]These studies were supported by the National Institutes of Health (Grant DK045686).

*To whom correspondence should be addressed. Telephone: (517) 884-5404. Fax: (517) 353-8957. E-mail: hausinge@msu.edu.

[1]Abbreviations: $UreG_{Str}$, UreG tagged with *Strep* II; CD, circular dichroism; DTT, dithiothreitol; HEPES, 4-(2-hydroxyethyl)-1-piperazineethanesulfonic acid; IPTG, isopropyl β-D-1-thiogalactopyranoside; MBP, maltose binding protein; MWCO, molecular weight cutoff; PCR, polymerase chain reaction; PAR, 4-(2-pyridylazo)resorcinol; SDS−PAGE, sodium dodecyl sulfate−polyacrylamide gel electrophoresis.

Published on Web 06/09/2010

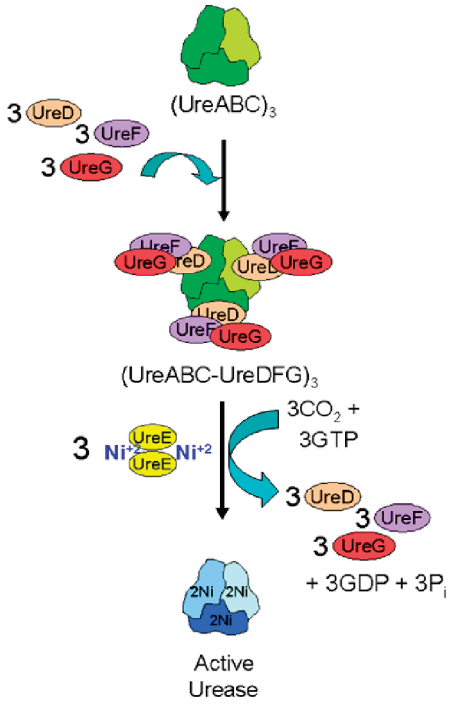

FIGURE 1: Simplified scheme of the urease activation process. Urease apoprotein $(UreABC)_3$ is synthesized with the nascent active site lacking nickel ions and with no carboxylation of its Lys217. Urease accessory proteins UreD, UreF, and UreG bind the apoprotein in a sequential manner to form the $(UreABC{-}UreDFG)_3$ activation complex. Urease activation requires carboxylation of Lys217 by CO_2, provision of nickel ions by the UreE metallochaperone, and GTP hydrolysis accompanied by release of the accessory proteins.

with the subunits joined by a disulfide bridge involving Cys68 in the *B. pasteurii* protein and probably Cys90 in that from *M. tuberculosis* (*21*, *23*). UreG from *B. pasteurii* binds two zinc ions per dimer (K_d 42 μM) or four nickel ions per dimer (K_d 360 μM), and this interaction was speculated to involve Glu64, Cys68 (i.e., the same residue as that participating in the disulfide), and His70 as metal ligands (*20*), although no experiments were performed to confirm these assignments. *H. pylori* UreG, a monomer as purified, dimerizes as it binds zinc ions (1.0 Zn per dimer, K_d 0.33 μM) or remains a monomer as it binds nickel ions with lower affinity (2.0 Ni per monomer, K_d 10 μM) (*22*). Cys66 and His68 are proposed as ligands for the zinc ion-binding site, but the C66A, H68A, and C66A/H68A double mutant still bind zinc with only 10-fold lower affinity, and these mutant proteins still dimerize upon addition of the metal ions. Furthermore, the presence of zinc, but not nickel, ions stabilizes a UreE−UreG complex using the *H. pylori* proteins (*24*). No crystal structure is available for any UreG; however, the crystal structure of the related protein HypB from *Methanocaldococcus jannaschii* is known (*25*). HypB is an accessory protein that participates in the metallocenter assembly of [NiFe] hydrogenases (*8*, *26*). The crystal structure reveals two types of zinc-binding sites: a mononuclear site in each subunit involving His100 and His104 (numbering derived from the HypB crystal structure; corresponding His residues are not located at these positions in UreG sequences) and a nonsymmetrical dinuclear binding site at the subunit interface. The metal-binding residues of the dinuclear site in *M. jannaschii* HypB (Cys95, His96, and Cys127) most likely correspond to Cys72, His74, and either Ser111 or Ser115 (although Ser is not a typical metal-binding residue) in *K. aerogenes* UreG (or Cys68, His70, and Ser107 or Ser111 in the *B. pasteurii* protein) (Figure 2).

UreE serves as a metallochaperone that delivers the nickel ions needed to form the urease active site (*27*, *28*). The structures of a truncated version of UreE from *K. aerogenes* and the full-length protein from *B. pasteurii* have been solved with bound copper and zinc, respectively (*29*, *30*). The interaction of UreE with the other accessory proteins has not been well characterized; however, UreE and UreG from *H. pylori* were suggested to interact on the basis of yeast two-hybrid assays (*31*), and a $UreE_2UreG_2$ complex (formed with the isolated *H. pylori* proteins) was observed in the presence of zinc, but not nickel, ions (*24*).

In this study, we describe a new purification method for UreG that utilizes a *Strep* tag. Using protein purified by this approach, we examine the metal-binding capabilities of $UreG_{Str}$ and a selection of its variants. Additionally, we assess the effects of those mutations on urease activation and exploit the *Strep*-tagged protein to examine its interactions with other urease components. Our findings using the *K. aerogenes* urease activation system expressed in *E. coli* reveal significant new insights, many of which are likely to be more generally applicable to other urease systems.

EXPERIMENTAL PROCEDURES

Vector Construction, Cell Growth, and Purification of Strep-Tagged UreG. The *ureG* sequence was cloned into pASK-IBA3plus and pASK-IBA5plus plasmids (IBA GmbH, Göttingen, Germany) to create vectors pIBA3+G and pIBA5+G (Supporting Information Table S1) encoding UreG with a *Strep* tag II (a WSHPQFEK peptide; subsequently referred to as a *Strep* tag) at the C- or N-termini, respectively. First, a polymerase chain reaction (PCR) was performed using *Pfu*Turbo Hotstart PCR master mix (Stratagene), the plasmid pKAUG-1 as a template, and the primers 5′-TA CTG TC*C CGC GG*G ATG AAC TCT TAT AAA CAC-3′ and 5′-T ACT GTC *CTG CAG* TTT GCC AAG CAT GCC TTT-3′. The first primer contains a *Sac*II restriction site and the second a *Pst*I restriction site (shown in italics) used to clone the fragment into pASK-IBA3plus. In a similar manner, the primers 5′-T ACT GTC *CCG CGG* GG AAC TCT TAT AAA CAC CCG-3′ and 5′- T ACT GTC *GGA TCC* CTA TTT GCC AAG CAT GCC-3′, containing restriction sites for *Sac*II and *Bam*HI, respectively, were used to clone the fragment into pASK-IBA5plus. The plasmids and PCR products were digested with the corresponding restriction enzymes (New England Biolabs) and ligated to produce plasmids pIBA3+G and pIBA5+G. These constructions were confirmed by sequencing (Davis Sequencing, Davis, CA).

Isolated colonies of *E. coli* BL21(DE3) (Stratagene) were transformed with the plasmids and grown at 37 °C overnight in lysogeny broth (LB, or Lennox broth; Fisher Scientific) supplemented with 300 μg mL^{-1} ampicillin. These cultures were used to inoculate 1 L of LB supplemented with 300 μg mL^{-1} ampicillin. The cultures were grown at 37 °C with shaking for 4 h and induced overnight with 0.2 μg mL^{-1} anhydrotetracycline. The cells were harvested by centrifugation and resuspended in 1 mL of buffer W (100 mM Tris-HCl, pH 8.0, containing 150 mM NaCl and 1 mM EDTA) per gram of cells and supplemented with 1 mM phenylmethanesulfonyl fluoride as a protease inhibitor before sonication (Branson 450 sonifier, five repetitions, each of 2 min, at 3 W output power and 50% duty cycle). The disrupted cells were centrifuged at 100000*g* at 4 °C for 45 min, and the cell-free supernatant was loaded onto a 1 mL *Strep*-Tactin column (IBA, Germany) previously equilibrated in buffer W. This column has an engineered streptavidin ligand that binds to the

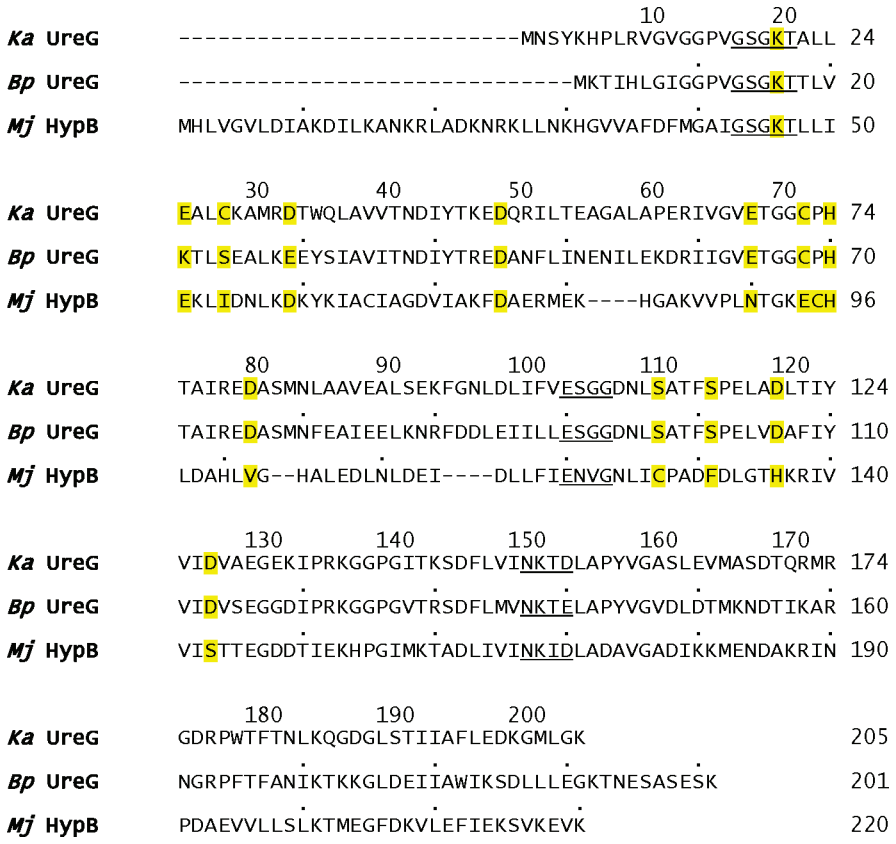

FIGURE 2: Multiple sequence alignment of *K. aerogenes* UreG, *B. pasteurii* UreG, and *M. jannaschii* HypB. Clustal W (*40*) was used to make the initial alignment, followed by manual modifications. Residues mutated in *K. aerogenes* UreG and the corresponding residues in the other sequences are highlighted in yellow. The P-loop motif, signature motif of the SIMBI G3E family, and guanine specificity loop are underlined.

Strep tag with high affinity. The *Strep*-tagged UreG protein ($UreG_{Str}$) was eluted with dethiobiotin according to the manufacturer's instructions. For comparative studies, native UreG was purified as previously described (*13*). For further purification and to provide assurance that samples were completely reduced, the proteins were chromatographed at 1 mL min^{-1} on a preparative Superdex-75 column (65 cm ×2.0 cm diameter; GE Healthcare) equilibrated in 50 mM HEPES buffer, pH 7.4, containing 200 mM NaCl, 1 mM EDTA and 1 mM dithiothreitol (DTT).

Fractions containing $UreG_{Str}$, UreG, or mutant forms of these proteins were analyzed by sodium dodecyl sulfate−polyacrylamide gel electrophoresis (SDS−PAGE) (*32*) using gels prepared with 12% running and 5% stacking acrylamide sections and stained with Coomassie brilliant blue. The calculated molecular masses of UreA (11.1 kDa), UreB (11.7 kDa), UreE (17.6 kDa), UreG (21.9 kDa), $UreG_{Str}$ (23.1 kDa), UreF (25.2 kDa), UreD (29.8 kDa), and UreC (60.3 kDa) generally migrate during electrophoresis as expected with the exception of UreG and $UreG_{Str}$, which behave as if they are larger than UreF. Molecular mass markers were obtained from Bio-Rad (Hercules, CA). Protein concentrations were determined by using a commercial dye-binding assay (Bio-Rad, Hercules, CA) with bovine serum albumin as the standard.

UreE Purification. *E. coli* DH5α cells containing pEC007 (*16*), expressing full-length UreE, were grown overnight in 10 mL of LB supplemented with 50 μg mL^{-1} chloramphenicol. These cultures were used to inoculate 1 L of LB supplemented with 50 μg mL^{-1} chloramphenicol and grown to an optical density at 600 nm (OD_{600}) of 0.4, induced with 0.5 mM isopropyl β-D-1-thiogalactopyranoside (IPTG), and grown overnight at 37 °C. UreE was purified by using previously published protocols (*33*).

Site-Directed Mutagenesis. pIBA3+G was mutated by using overlapping oligonucleotides containing the desired mutation (see Supporting Information Table S2) during PCR performed with *Pfu*Turbo Hotstart PCR master mix. The products were digested with *Dpn*I for 1 h at 37 °C and used to transform chemically competent *E. coli* DH5α cells. After confirmation by sequencing, the mutated plasmids were transformed into *E. coli* BL21(DE3) competent cells (Stratagene). All mutant $UreG_{Str}$ proteins were expressed and purified as described for $UreG_{Str}$.

Circular Dichroism (*CD*). Wild-type and *Strep*-tagged UreG proteins were purified and concentrated up to 0.2 mg mL^{-1} in 15 mM potassium phosphate buffer, pH 7.6, containing 1 mM DTT. A 100 μL sample was placed into a 1 cm path length cell and scanned using a Jasco J-710 spectropolarimeter between 180 and 300 nm. The data were analyzed with the DICHROWEB server (*34*), and the best fit was obtained by using CDSSTR and set 4.

Analytical Gel Filtration Chromatography. Analytical hydrodynamic radius assays used Sephacryl 300 HR (65 cm ×2.0 cm diameter; Sigma). The buffer contained 50 mM HEPES, pH 7.4, with 200 mM NaCl and other additives as indicated, using a flow rate of 1 mL min^{-1}.

In Vivo Expression of $UreG_{Str}$ Variants in the Context of the Urease Operon. Plasmid pKK17 (*27*), which contains the entire *ureDABCEFG* urease gene cluster under the control of the *tac* promoter, was modified to encode $UreG_{Str}$ and its mutant forms by replacing a *Psi*I/*Kpn*I fragment to create plasmid pKKG and variants. For analysis of urease activity in cell extracts, *E. coli* DH5α containing the desired plasmid was inoculated into 1 mL of LB supplemented with 300 μg mL^{-1} ampicillin and 1 mM $NiCl_2$

(unless noted) and grown overnight at 37 °C with agitation. A 0.25 mL aliquot of the culture was used to inoculate 25 mL of LB containing 100 μg mL^{-1} ampicillin plus 1 mM $NiCl_2$ (unless noted) and grown for 2.5 h at 37 °C with agitation. IPTG added to 0.1 mM was used to induce the expression of the operon overnight at 37 °C. Cells were harvested by centrifugation for 10 min at 5000*g* and 4 °C and resuspended in either 1 mL of 25 mM HEPES buffer, pH 7.4, if performing urease activity assays or 750 μL of buffer W if used for pull-down assays. Phenylmethanesulfonyl fluoride was added to 0.1 mM, the cells were sonicated (Branson 450 sonifier, five repetitions, each of 45 s, at 1 W output power and 50% duty cycle), and the disrupted cells were centrifuged for 10 min at 4 °C and 16000*g* in a microcentrifuge. The soluble, cell-free extracts were used to test urease activity and perform pull-down assays.

Urease Activity Assays. Urease activities were measured by quantifying the rate of ammonia release from urea by formation of indophenol, which was monitored at 625 nm (*35*). One unit of urease activity was defined as the amount of enzyme required to hydrolyze 1 μmol of urea/min at 37 °C. The standard assay buffer consisted of 50 mM HEPES, pH 7.8, and 50 mM urea.

Metal Quantification. The metal contents of freshly purified UreG and $UreG_{Str}$ were assessed by using inductively coupled plasma-emission spectrometry at the University of Georgia Chemical Analysis Laboratory.

Metal Binding Analyses. Purified proteins were dialyzed overnight against 50 mM HEPES buffer, pH 7.4, containing 200 mM NaCl, 1 mM EDTA, and 1 mM DTT, followed by dialysis against 50 mM HEPES buffer, pH 7.4, containing 200 mM NaCl until the EDTA and DTT concentrations were negligible. Nonradioactive equilibrium dialysis experiments were performed by using an equilibrium microvolume dialyzer (Hoefer Scientific instruments). Purified protein (400 μL of 10 μM) was dialyzed against 400 μL of various concentrations of $NiCl_2$ or $ZnCl_2$ overnight at 4 °C by using a 3500 Da molecular mass cutoff membrane (MWCO; Spectra-Por). Metal concentrations on both sides of the membrane were determined by adding 100 μL of these solutions to 900 μL of 100 μM 4-(2-pyridylazo)resorcinol (PAR) made in 50 mM HEPES (pH 7.4) with 200 mM NaCl, incubating for 10 min, and monitoring the absorbance at 500 nm (*36*). The data were plotted and analyzed in Sigma Plot (Systat Software, Inc.) by using eq 1, appropriate for samples containing a single type of binding site, where Y is the number of metal ions bound per UreG subunit, B_{max} is the maximum number of metal ions bound per UreG peptide, $[M_f]$ is the concentration of free metal ions, and K_d is the dissociation constant.

$$Y = B_{max}[M_f]/(K_d + [M_f]) \quad (1)$$

Metal competition experiments were performed in a rapid equilibrium dialysis plate (Pierce Biotechnology, Rockford, IL). Purified $UreG_{Str}$ (300 μL of 25 μM) was dialyzed against 500 μL of varying concentrations of nickel ions containing ^{63}Ni and the indicated concentrations of $ZnCl_2$, with shaking overnight at 5 °C and 300 rpm. Aliquots of the resulting samples (200 μL) were added to 10 mL of Safety Solve (Research Products International Corp.), and ^{63}Ni contents were determined by using a Beckman-Coulter LS6500 liquid scintillation counter. The data were fit by using the following equation for competitive binding to a single type of binding site:

$$Y = B_{max}[Ni]/\{K_d(1 + [Zn]/K_i) + [Ni]\} \quad (2)$$

The constants are as indicated above, and K_i is the inhibition constant for Zn.

UV−Visible Spectroscopy. Samples (1 mL) of the indicated concentrations of $UreG_{Str}$, C28A $UreG_{Str}$, and C72A $UreG_{Str}$ in 50 mM HEPES, pH 7.4, containing 200 mM NaCl were titrated with aliquots of 1−5 μL of 1 mM $NiCl_2$. Absorption spectra were obtained after each addition, and these were corrected for dilution.

Pull-Down Assays. Soluble cell-free extracts from *E. coli* DH5α containing pKKG grown with and without supplemented Ni were loaded onto a 0.3 mL *Strep*-Tactin column equilibrated in buffer W. Proteins were eluted according to the manufacturer's instructions and analyzed by using 13.5% SDS−PAGE.

For *in vitro* pull-down assays, UreE and $UreG_{Str}$ or variants were mixed in a final concentration of 16 μM for each protomer with varying concentrations of $NiCl_2$ or $ZnCl_2$, incubated on ice as indicated, applied to a 0.5 mL *Strep*-Tactin column, washed, and eluted according to the manufacturer's instructions. Eluted fractions were analyzed by using 12% SDS−PAGE. Further analysis of the interaction between UreE and $UreG_{Str}$ was carried out by mixing equal concentrations of each protein (40 or 150 μM protomer) and subjecting the mixture to chromatography on Sephacryl S-300 in buffer containing or lacking 60 μM $NiCl_2$.

Western Blot. Proteins were resolved by SDS−PAGE and transferred to an Immobilon-P polyvinylidene difluoride membrane (Millipore). ExtrAvidin−alkaline phosphatase conjugate (1:2500 dilution; Sigma) was used as a probe to bind to *Strep*-tagged forms of UreG. BCIP/NBT-Blue liquid substrate (Sigma) was added to develop the color. To detect UreE or urease, the membranes were incubated for 45 min with anti-UreE IgG (1:10000 dilution) (*33*) or anti-urease antibody (1:5000 dilution) (*37*) in TBS buffer (150 mM NaCl, 100 mM Tris, pH 7.4) containing 1% Tween 20. After the membranes were washed four times with TBS buffer, they were incubated for 45 min with anti-rabbit IgG conjugated to alkaline phosphatase (Sigma) that was diluted 30000-fold. The membranes were washed again, and BCIP/NBT-Blue liquid substrate was added to develop the color. Prestained molecular mass markers were obtained from Bio-Rad (Hercules, CA).

RESULTS

Characterization of Strep-Tagged UreG. The native form of *K. aerogenes* UreG was previously purified from recombinant *E. coli* cells by sequential use of two Mono-Q columns in different buffers followed by gel filtration chromatography (*13*); however, the tendency of the protein to elute from ion-exchange resins over a large number of fractions led to low overall yields. To overcome this problem and to facilitate a single-step purification of UreG variants, we developed a new purification system exploiting a fusion peptide sequence that binds with high affinity to *Strep*-Tactin resin. The *Strep* tag II (*38*, *39*) was designed specifically to allow affinity purification without introduction of metal-binding residues as in the commonly used His_6 tag. The *ureG* sequence was cloned into plasmids pASK-IBA3plus and pASK-IBA5plus to encode UreG fused with a *Strep* tag at the C- and N-terminus, respectively. *E. coli* BL21(DE3) cells transformed with the plasmid derived from the pASK-IBA3plus vector produced more recombinant protein, so this plasmid was selected for further experiments. For comparative analyses, native UreG also was obtained by using the previously described protocol (*13*).

Highly purified $UreG_{Str}$ was obtained by single-step chromatography on a *Strep*-Tactin column, and essentially homogeneous protein was available after subsequent gel filtration

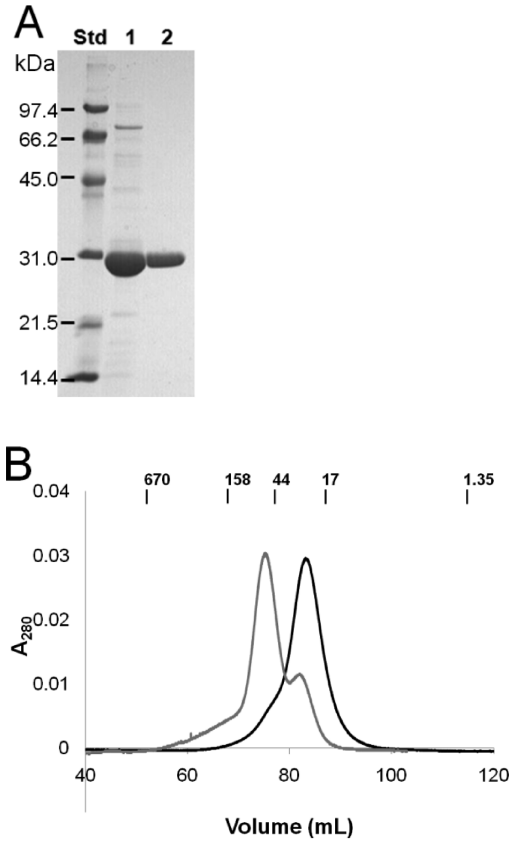

FIGURE 3: Purification of $UreG_{Str}$ and size exclusion chromatography native size analysis. (A) Purification of $UreG_{Str}$. Lane 1: $UreG_{Str}$ after *Strep*-Tactin column purification. Lane 2: $UreG_{Str}$ after Superdex-75 gel filtration chromatography. (B) Sephacryl S300HR size exclusion chromatography. $UreG_{Str}$ (1.0 mL) was loaded onto a 130 mL Sephacryl S-300 column equilibrated with 50 mM HEPES buffer, pH 7.4, containing 200 mM NaCl plus 15 μM $NiCl_2$ and chromatographed at a flow rate of 1 mL min^{-1}. Black: $UreG_{Str}$. Gray: C28A $UreG_{Str}$. The positions of molecular mass standards (Bio-Rad) are indicated in kDa.

chromatography in buffer containing 1 mM DTT (Figure 3A). The elution profile (Figure 3B) was consistent with $UreG_{Str}$ being monomeric with a very small shoulder suggesting a trace of dimeric protein. Significantly, the monomeric nature of this protein was retained regardless of the presence or absence of nickel or zinc ions. By contrast to these metal ion-independent results, the inclusion of nickel ions caused the C28A $UreG_{Str}$ variant to chromatograph primarily as a dimer (Figure 3B, gray trace), as described further in a later section. For comparison to $UreG_{Str}$, native UreG exhibited a major monomeric species as well as a minor dimeric feature by size exclusion chromatography (data not shown), with the dimer peak disappearing after overnight dialysis in a buffer containing DTT. These results are consistent with the dimer being an artifact of oxidation that occurs much more readily in the wild-type protein than in $UreG_{Str}$.

The presence of the *Strep* tag did not affect folding of UreG according to CD spectroscopy (spectra not shown). Fitting of the spectra indicated $UreG_{Str}$ (60% α helix, 18% β strands, 4% turns, and 18% random coil for $UreG_{Str}$) possessed essentially the same secondary structure as native UreG (65% α helix, 15% β strands, 5% turns, and 15% random coil for native UreG), each with a normalized root-mean-square deviation of 0.001.

Targeting Residues for Mutagenesis. Several criteria were used to select $UreG_{Str}$ residues for mutagenesis. First, we identified highly conserved residues by creating an alignment using Clustal W (*40*) of the most diverse UreG and HypB sequences found in the NCBI database along with other UreG sequences of interest. The hydrogenase-activating GTPases are ~25% identical in sequence to UreG, and both of these protein families function in assembly of nickel metallocenters. Notably, residues conserved in these two protein families constitute a much smaller number than the residues conserved in just UreG proteins (where the identities typically are over 50%; see UreG sequence comparisons in refs *20* and *21*). The UreG/HypB sequence comparison highlights the P-loop motif (GSGKT at positions 17−21 in *K. aerogenes* UreG), the signature motif (ESGG at positions 104−107 of UreG) for the SIMBI G3E family of GTPases (*41*), and the guanine specificity loop (NKTD at positions 151−154 of UreG) (Figure 2). Second, we examined the crystal structure of *M. jannaschii* HypB (*25*) which uses Cys95, His96, and Cys127 to coordinate a dinuclear zinc-binding site; counterparts were identified in *K. aerogenes* UreG (Cys72, His74, and perhaps either Ser111 or Ser115, although Ser is rarely observed as a metal ligand). In addition, the HypB structure indicated multiple residues involved in MgGTP binding, hinting at the comparable residues in UreG. Finally, we identified *K. aerogenes* UreG residues corresponding to those hypothesized to be metal ligands in *B. pasteurii* UreG (*20*), as well as some residues that were not as highly conserved but seemed likely choices for metal binding.

On the basis of these criteria, the following residues were targeted for mutagenesis. Lys20, previously shown to be a critical P-loop residue (*13*), was changed to form K20A $UreG_{Str}$. Asp49, equivalent to the Mg^{2+}-coordinating Asp75 in *M. jannaschii* HypB (*25*), was changed to generate D49A $UreG_{Str}$. Glu68, the residue corresponding to a suggested metal ligand of the *B. pasteurii* protein (*20*), was changed to obtain the E68A protein. Cys72, likely to correspond to the Cys95 metal ligand at the dinuclear site of *M. jannaschii* HypB (*25*) and whose equivalent was speculated to be a metal ligand in *B. pasteurii* UreG (*20*), was changed to create the C72A variant. His74, likely to correspond to the His96 dinuclear center ligand of HypB (*25*) and equivalent to the postulated His70 metal ligand in *B. pasteurii* UreG (*20*), was changed to produce the H74A mutant protein. Asp80, corresponding to Asp98 of HypB (where it is positioned between the dinuclear center and the GTP-binding site) and highly conserved in both proteins, was changed to make D80A $UreG_{Str}$. Ser111 and Ser115 that approximate the Cys127 ligand of the dinuclear site in HypB were changed to fashion the S111A and S115A proteins. In addition, Cys28, the only other cysteine residue in the *K. aerogenes* UreG sequence, along with Glu25 and Asp33, the two acidic residues closest to that cysteine, and Asp120 and Asp127, two highly conserved aspartic acid residues, were all changed to alanine residues.

Effect of $UreG_{Str}$ Variants on Urease Activity in Cell Extracts. The selected *ureG* mutants were expressed as part of the urease operon, and the levels of the encoded $UreG_{Str}$ variants were shown to be indistinguishable by Western blot (data not shown). The urease activities measured in soluble extracts of cells producing $UreG_{Str}$ were essentially identical to those of extracts from cells containing native UreG (Table 1). Similarly, cell-free extracts containing D33A and E68A $UreG_{Str}$ possessed about 80% of the activity observed for extracts containing the non-mutant $UreG_{Str}$. The E25A, C28A, S115A, and D127A forms of $UreG_{Str}$ exhibited somewhat diminished activities (5%, 13%, 30%, and 33%, respectively, of wild-type urease activity). In contrast, the cells producing K20A, D49A, C72A, H74A, D80A, and S111A variants of $UreG_{Str}$ exhibited nearly undetectable

Table 1: Effects of UreG Mutations on Urease Activity in Soluble Cell-Free Extracts

sample	specific activity (units mg^{-1})[a]	specific activity (% of wild type)
UreG	129.6 ± 10.4	100
UreG$_{Str}$	122.6 ± 9.8	94.6
K20A UreG$_{Str}$	0.09 ± 0.01	0.07
E25A UreG$_{Str}$	6.4 ± 1.9	4.94
C28A UreG$_{Str}$	16.6 ± 1.3	12.8
D33A UreG$_{Str}$	105.4 ± 10.5	81.3
D49A UreG$_{Str}$	0.19 ± 0.04	0.15
E68A UreG$_{Str}$	107.4 ± 8.6	82.9
C72A UreG$_{Str}$	0.14 ± 0.02	0.11
H74A UreG$_{Str}$	0.14 ± 0.04	0.11
D80A UreG$_{Str}$	0.24 ± 0.15	0.19
S111A UreG$_{Str}$	0.09 ± 0.01	0.07
S115A UreG$_{Str}$	39 ± 10	30.1
D127A UreG$_{Str}$	42.6 ± 6.2	32.9

[a]Error values are standard deviation from triplicate biological samples, including a minimum error associated with protein assays.

Table 2: Thermodynamics of Nickel Ion Binding to UreG, UreG$_{Str}$, and Its Variants

protein	K_d (μM)	B_{max}
UreG	16 ± 3.1	1.0 ± 0.08
UreG$_{Str}$	5.0 ± 1.8	0.95 ± 0.09
E25A UreG$_{Str}$	18 ± 5	0.75 ± 0.08
C28A UreG$_{Str}$	8.5 ± 1.9	0.81 ± 0.06
D49A UreG$_{Str}$	11 ± 2	0.94 ± 0.08
E68A UreG$_{Str}$	7.7 ± 3.3	0.82 ± 0.09
C72A UreG$_{Str}$	61 ± 13	1.21 ± 0.1
H74A UreG$_{Str}$	12 ± 4	1.2 ± 0.1
D80A UreG$_{Str}$	20 ± 9	1.1 ± 0.1
S111A UreG$_{Str}$	6.6 ± 2.4	0.97 ± 0.1
S115A UreG$_{Str}$	12 ± 4	1.1 ± 0.1
D120A UreG$_{Str}$	10 ± 2	0.92 ± 0.06
D127A UreG$_{Str}$[a]	10 ± 5	1.5 ± 0.2

[a]Data were obtained for this sample using a 15000 MWCO membrane, whereas all other data used a 3500 MWCO membrane.

levels of urease activity. For unidentified reasons, the gene encoding D120A UreG$_{Str}$ was unable to be cloned into the urease gene cluster despite repeated attempts.

Metal Binding to UreG, UreG$_{Str}$, and UreG$_{Str}$ Variants. Based on published metal-binding studies of UreG from other sources (*20*−*23*) and the dinuclear zinc metallocenter structure of HypB, we tested whether UreG from *K. aerogenes* would bind nickel or zinc ions. Freshly purified UreG and UreG$_{Str}$ were free of metal according to inductively coupled plasma-emission spectrometry. The nickel and zinc ion-binding properties of UreG, UreG$_{Str}$, and the site-directed mutants were examined by using PAR, a colorimetric indicator (*36*), to monitor metal concentrations after equilibrium dialysis (Table 2). As shown in Figure 4, UreG$_{Str}$ and native UreG each bound approximately one nickel ion per monomer (1.0 ± 0.08 and 0.95 ± 0.09 per monomer, respectively), with UreG$_{Str}$ also binding 1.1 ± 0.08 Zn (zinc ion binding to native UreG could not be reliably determined due to protein precipitation). Surprisingly, UreG$_{Str}$ bound nickel ions with greater affinity (K_d = 5.0 ± 1.8 μM) than native UreG (K_d = 16 ± 3.1 μM) (Figure 4A). The basis of this lower K_d is unclear, and this difference in K_d could be a point of potential concern; however, UreG$_{Str}$ is able to activate urease to wild-type levels (Table 1).

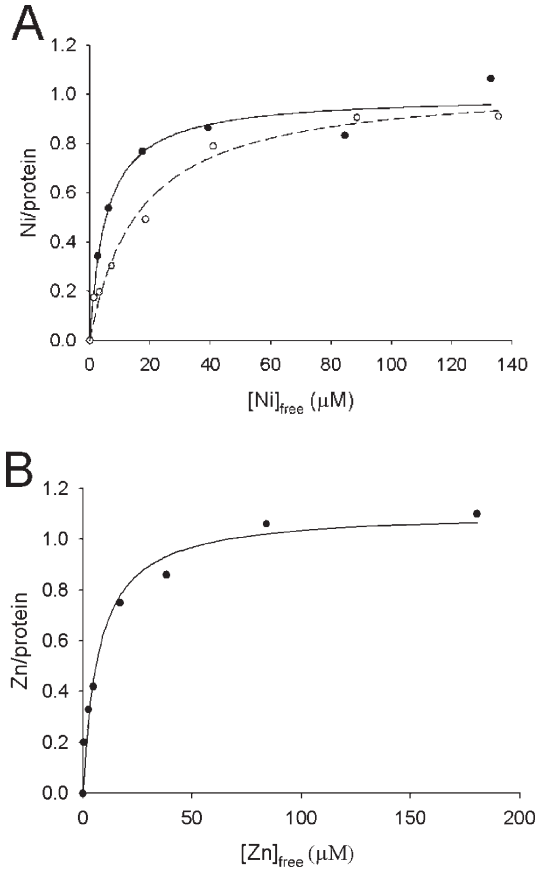

FIGURE 4: Equilibrium dialysis analysis of metal binding to wild-type and *Strep*-tagged UreG. (A) Nickel ion binding to UreG$_{Str}$ (filled circles) and UreG (open circles). (B) Zinc ion binding to UreG$_{Str}$. The concentrations of metal ions in dialysis chambers containing protein and buffer were assessed by reaction with PAR, and the differences of these values were used to calculate the amounts of metal−protein complexes. Ligand binding fits to a single type of binding site are indicated.

Thus, the nickel-binding properties of the variant proteins were studied by using the tagged constructs, and selected results were confirmed by using the nontagged version.

In order to examine whether nickel and zinc ions compete for the same metal-binding site of UreG$_{Str}$, additional equilibrium dialysis experiments used ^{63}Ni. When dialyzed against varying concentrations of nickel ions containing ^{63}Ni, UreG$_{Str}$ (25 μM) bound 1.15 ± 0.07 nickel ions per monomer with a K_d of 2.7 ± 0.2 μM (Figure 5A), in very reasonable agreement with the PAR data. Using these baseline data, two types of competitive binding assays were performed. First, UreG$_{Str}$ was dialyzed against varying concentrations of nickel ions containing ^{63}Ni and a constant concentration of zinc ions (10 μM) (Figure 5A, dashed line). These results clearly demonstrate competition between the metal ions; eq 2 provided a zinc ion K_i of 3.9 ± 0.3 μM. Second, UreG$_{Str}$ was dialyzed against a constant concentration of nickel ions (25 μM) containing ^{63}Ni along with varied concentrations of zinc ions (Figure 5B). A zinc ion K_i of 2.7 ± 0.2 μM was determined, in close agreement with the first method. The K_i for zinc ion competition of nickel ion binding is in good agreement with the K_d for Zn determined by the PAR method (Figure 4B).

PAR-based equilibrium dialysis experiments were carried out with all site-directed variants. Unfortunately, zinc ions caused protein precipitation at concentrations higher than 100 μM with nearly all of the mutant UreG$_{Str}$ proteins, thus precluding their detailed thermodynamic analyses. In contrast, the mutant proteins

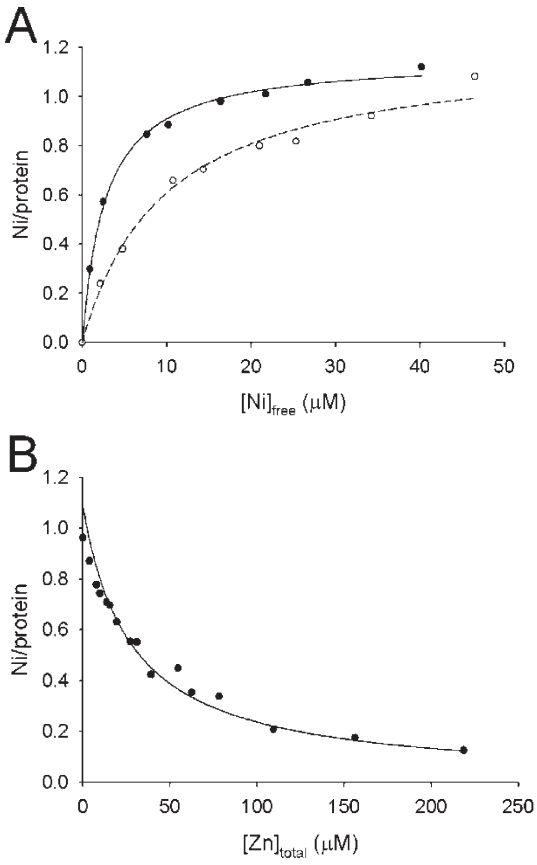

FIGURE 5: Equilibrium dialysis analyses to assess the competition of nickel and zinc ions. (A) Varying concentrations of nickel ions containing ^{63}Ni were examined for binding to 25 μM UreG$_{Str}$ in the absence of added zinc ions (filled circles) or in competition with 10 μM $ZnCl_2$ (open circles). (B) 25 μM UreG$_{Str}$ was mixed with 25 μM nickel ions containing ^{63}Ni and varied concentrations of zinc ions. The data were fit by using eq 2.

exhibited well-behaved nickel ion-binding curves. Table 2 provides the nickel ion K_d and B_{max} for each mutant protein. Most UreG$_{Str}$ variants behaved much like the control protein in terms of their thermodynamics of nickel ion binding. That is, their K_d values were the same or only slightly larger than that of UreG$_{Str}$, and they bound a single nickel ion per protomer. Nearly 4-fold increases in K_d were measured with the E25A and D80A variants. The largest change in thermodynamic properties was measured in the case of the C72A UreG$_{Str}$ variant, which exhibited a nickel ion K_d of 61 $\pm$ 13 μM, consistent with its involvement in metal binding. Parallel to the large increase in K_d for C72A UreG$_{Str}$ compared to UreG$_{Str}$, a similar large increase in K_d was demonstrated in the mutant protein lacking the *Strep* tag (59 $\pm$ 24 μM; data not tabulated). By contrast to the results related to substitution of Cys72, the mutation affecting the only other Cys in the protein (i.e., C28A UreG$_{Str}$) behaved much like the control protein in terms of its thermodynamic properties. Nevertheless, this protein did exhibit anomalous behavior. In particular, the C28A variant formed predominantly a dimer in the presence of nickel ions as identified by gel filtration chromatography experiments (Figure 3B).

In order to further investigate the nature of the nickel ion-binding site in UreG, $NiCl_2$ was titrated into solutions of UreG$_{Str}$ and the two UreG$_{Str}$ cysteine variants while monitoring their UV−visible spectra. For UreG$_{Str}$, a peak at 330 nm appeared with increasing Ni^{2+} concentrations (Figure 6A). This feature is consistent with a thiolate-to-Ni^{2+} charge-transfer transition (*42*); however, the changes in intensity of this peak versus the concentrations of added nickel ions (Figure 6C) do not fit the behavior expected for a single metal ion-binding event and were inconsistent with the K_d obtained by equilibrium dialysis analysis, indicating that the two techniques are not reporting on the same event. No absorption feature was detected when nickel ions were added to the C72A protein (data not shown), indicating that Cys72 is primarily responsible for the ligand-to-metal charge-transfer band noted for UreG$_{Str}$. Titration of nickel ions into the C28A UreG$_{Str}$ protein yielded a feature at 303 nm (Figure 6B). The perturbation of the peak maximum compared to that of the nonmutated protein could be indicative of a different ligand environment for the metal ion in the primarily dimeric C28A UreG$_{Str}$. The intensity changes observed for the C28A variant with varied nickel ion concentrations (Figure 6D) do not saturate as the metal ion concentrations increase and thus do not reflect the expectations from equilibrium dialysis, again consistent with the two methods measuring nonequivalent nickel ion-binding events. Regardless, it is clear that a Cys residue binds nickel ions in the C28A and native proteins but not in the C72A variant.

Pull-Down Assays. We exploited the *Strep* tag on UreG$_{Str}$ to examine the interactions of UreG with other cellular proteins and to identify complexes that form *in vivo*. *E. coli* DH5α cells containing the modified urease operon expressing UreG$_{Str}$ or mutants of this protein were grown with or without added nickel ions; then soluble cell-free extracts were chromatographed on *Strep*-Tactin columns and the proteins eluted with dethiobiotin-containing buffer. The resulting samples were examined by SDS−PAGE, with three key results illustrated (Figure 7). For most samples, UreG$_{Str}$ (the expected major band) associated with the urease structural subunits (identified by their characteristic sizes and by Western blot analysis using anti-urease antibodies; data not shown) along with bands migrating at positions expected for the UreD and UreF accessory proteins. In addition, Western blot analysis using anti-UreE antibodies (data not shown) identified UreE in all samples, but this protein was present in much smaller amounts for cells grown in the absence of added nickel ions. In contrast to the other samples, added nickel ions led to the D80A UreG$_{Str}$ forming a complex only with UreE and not associating with urease, UreD, or UreF (Figure 7A).

To further investigate the interaction between UreG$_{Str}$ and UreE, *in vitro* pull-down studies were performed with the purified proteins. UreG$_{Str}$ and UreE (1:1 molar ratio of protomers, 16 μM each) were mixed in buffer containing various concentrations of nickel or zinc ions. After being incubated approximately 10 min on ice, the samples were loaded onto *Strep*-Tactin columns and washed, and the bound proteins were eluted with dethiobiotin and examined by SDS−PAGE. An increasing ratio of UreE bound to UreG$_{Str}$ as the nickel or zinc ion concentrations increased, with approximately 0.5 UreE protomer per UreG observed for 60 μM or higher metal ion concentration according to densitometry measurements (Figure 7B). To test whether the amount of complex formation increased over time, a mixture of UreG$_{Str}$, UreE, and nickel ions was incubated on ice for up to 4 h before performing the pull-down experiment; all incubation times exhibited the same amount of complex (data not shown). The resulting UreG$_{Str}$−UreE complex was further investigated by using gel filtration chromatography. When equal protomer concentrations of the two proteins were combined and chromatographed on a Sephacryl S-300 column in the absence of metal ions (Figure 7C), a single feature was observed corresponding to overlapping peaks of the monomer of UreG$_{Str}$ (M_r = 23.1 kDa) and the dimer of UreE (M_r = 35.1 kDa). By contrast, when the

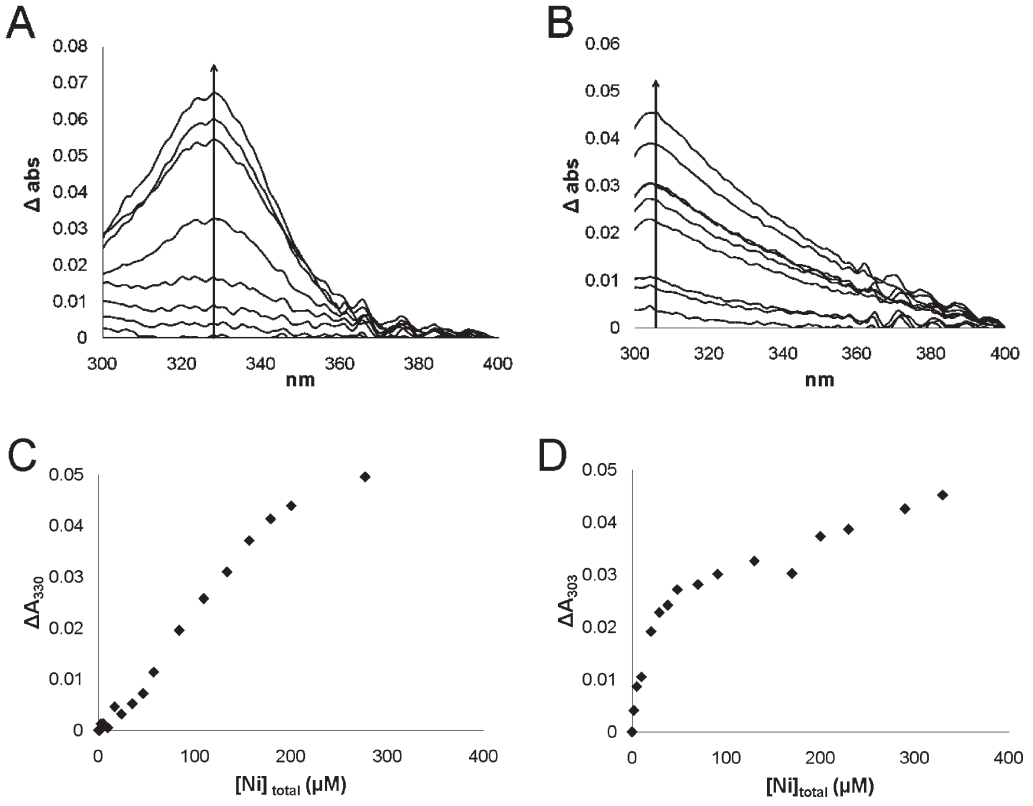

FIGURE 6: UV−visible spectral titrations of $UreG_{Str}$ and its C28A variant with $NiCl_2$. (A) Difference spectra obtained for 58 μM $UreG_{Str}$ titrated with nickel ions in 50 mM HEPES buffer, pH 7.4, containing 200 mM NaCl. (B) Difference spectra of 26 μM C28A $UreG_{Str}$ titrated with nickel ions in the same manner. (C) Difference in absorbance at 330 nm for $UreG_{Str}$ plotted against the total nickel ion concentration. (D) Difference in absorbance at 303 nm for C28A $UreG_{Str}$ plotted against total nickel ion concentration.

experiment was repeated with 60 μM $NiCl_2$ added to the buffer, a second peak with an apparent molecular mass of 168 kDa appeared. Analysis of fractions from that peak by using SDS−PAGE revealed an approximate 1:2 $UreG_{Str}$:UreE protomer ratio as calculated by using densitometry measurements (Figure 7D). Significantly, the ratio obtained here reflects the actual protomer ratio in the isolated complex, whereas the ratio described above includes a combination of UreE that reversibly associated with $UreG_{Str}$ as well as free $UreG_{Str}$. The second peak eluting from this column was comprised of predominantly $UreG_{Str}$ and chromatographed as the expected monomer. UreE alone forms an even larger complex with an apparent molecular mass of more than 330 kDa when 60 μM $NiCl_2$ is present (data not shown).

The $UreG_{Str}$ variants also were mixed with UreE and subjected to pull-down experiments. None of the $UreG_{Str}$ variants exhibited deficiencies in their abilities to form a complex with UreE when 60 μM nickel ions were present, nor did any of the mutations form a complex with UreE in the absence of metal.

DISCUSSION

Using a new procedure to purify *K. aerogenes* UreG, we generated significant findings related to the protein's functional quaternary structure, its metal ion-binding properties, the effects of selected mutations on activity and metal binding, and the formation of a complex between this protein and its cognate UreE in a manner induced by metal ions. Notably, some of these results obtained using *K. aerogenes* UreG exhibit stark differences compared to those reported for UreG proteins from other organisms (*20*−*22*).

The use of a *Strep* tag on UreG facilitated purification and allowed for protein interaction studies via pull-down assays. While designed to not interfere with metal-binding analyses (*38*, *39*), a major concern for the more widely used His_6 tag, we found the *Strep*-tagged version of UreG bound nickel ions more tightly than the wild-type protein. The basis of the 3-fold difference in K_d is unclear, but we note that the *Strep* tag contains a His residue which could play some role in metal binding or in slightly perturbing the protein conformation. These results demonstrate that any tag might have unexpected effects. Significantly, the tag on UreG does not interfere with its function in urease activation as shown by the ability of $UreG_{Str}$ to activate urease apoprotein within cells to 95% of that of the wild-type protein, signifying that the difference in the K_d does not affect the role of UreG *in vivo*.

CD measurements confirmed that the *Strep* tag did not interfere with the overall fold of the UreG protein. Furthermore, both wild-type UreG and $UreG_{Str}$ were found to be highly structured (only 18% and 15% random coil, respectively) compared to the intrinsically disordered structures of the *B. pasteurii*, *M. tuberculosis*, and *H. pylori* proteins (30%, 45%, and ~50% random coil, respectively) (*21*−*23*). This result might imply that *K. aerogenes* UreG is better suited for structural characterization efforts than UreG from other sources.

$UreG_{Str}$ is monomeric according to gel filtration experiments, and this state is unaffected by the addition of nickel or zinc ions. This quaternary structure differs from the dimeric UreG proteins of *B. pasteurii* or *M. tuberculosis* (*21*, *23*) and from *H. pylori* UreG which dimerizes in the presence of zinc, but not nickel, ions (*22*). Several other members of the SIMBI G3E family of small GTPases possess dimeric structures, while others are monomeric. For example, HypB and MeaB (an editor for transferring vitamin B_{12} into methylmalonyl-CoA mutase) crystallized as dimers, although, of potential interest, their dimer interfaces are distinct, whereas YjiA (a protein of undefined function) is a monomer (*25*, *43*−*45*).

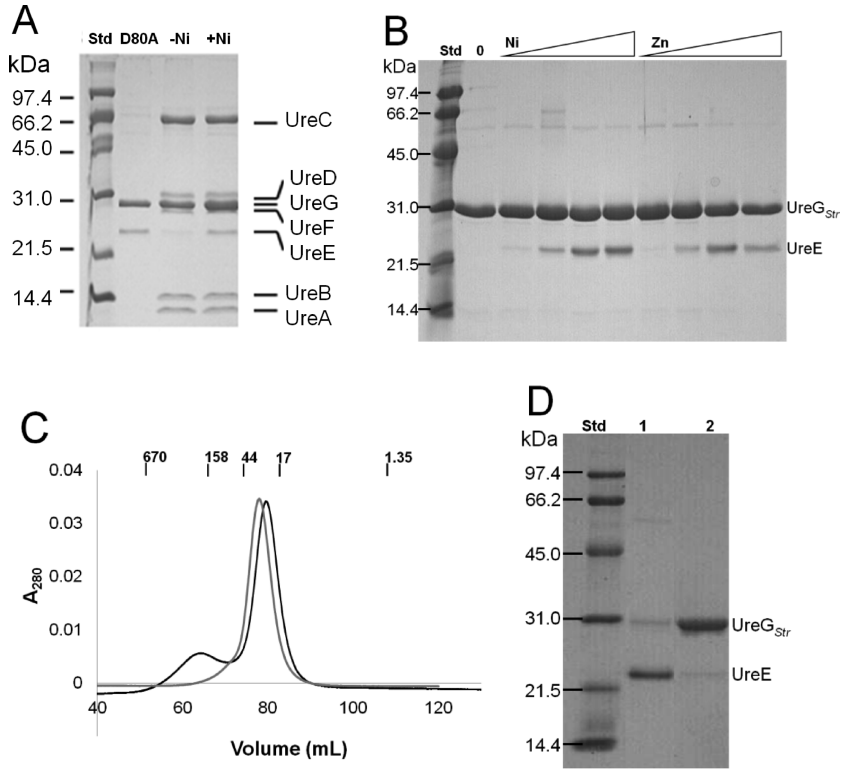

FIGURE 7: *In vivo* interactions of UreG$_{Str}$ with urease proteins and *in vitro* interactions between UreG$_{Str}$ and UreE. (A) *In vivo* complexes formed with selected UreG$_{Str}$ samples in *E. coli* DH5α cells. Soluble cell-free extracts were generated from cells grown in medium lacking (−Ni) or containing (+Ni) nickel ions and expressing the urease operon encoding nonmutated UreG$_{Str}$ or for cells expressing the operon encoding D80A UreG$_{Str}$ (+Ni). The extracts were applied to *Strep*-Tactin columns, and the proteins eluted with dethiobiotin were subjected to SDS−PAGE. (B) *In vitro* pull-down assays using purified UreG$_{Str}$ and UreE. The two proteins (1:1 molar ratio of protomers, 16 μM each) were incubated with varying concentrations of nickel or zinc ions (0−100 μM), loaded onto *Strep*-Tactin columns, eluted with dethiobiotin, and subjected to SDS−PAGE. (C) Sephacryl S-300 chromatography of a mixture of UreG$_{Str}$ and UreE (1:1 molar ratio of protomers) in 50 mM HEPES buffer, pH 7.4, containing 200 mM NaCl with (black) and without (gray) 60 μM $NiCl_2$. Molecular mass standards (Bio-Rad) are indicated in kDa. (D) SDS−PAGE analysis of the two peak fractions from the chromatograph of panel C that includes nickel ions.

Our conclusion that UreG functions as a monomeric protein in *K. aerogenes* coincides with earlier results indicating stoichiometric levels of UreD, UreF, and UreG in various urease complexes generated in this system and with data demonstrating that UreD and UreF are stoichiometric with the urease subunits (*11*−*13*, *16*, *46*).

The metal-binding properties of *K. aerogenes* UreG$_{Str}$ also differ significantly from those of UreG proteins isolated from other species. Equilibrium dialysis studies demonstrated that nickel and zinc ions compete with similar affinities for a single metal ion-binding site on UreG$_{Str}$. While the dimeric *B. pasteurii* UreG similarly binds one zinc ion per protomer, it binds two nickel ions per protomer with the affinities for the two metal ions differing by an order of magnitude (and these affinities are approximately 10- and 100-fold less than for *K. aerogenes* UreG$_{Str}$) (*20*). *H. pylori* UreG binds only 0.5 zinc ion per protomer leading to dimerization, whereas it binds two nickel ions per monomer without dimerization and with 20-fold lower affinity (*22*). In comparison to the *B. pasteurii* and *H. pylori* proteins, the small nickel ion K_d of UreG$_{Str}$ may be compatible with its functional significance in transferring nickel ions to UreD in the UreABC−UreDFG activation complex; however, one must be cautious in interpreting these thermodynamic results since urease metallocenter assembly is, at least in part, a kinetic process linked to GTP hydrolysis. Furthermore, we cannot rule out that the physiologically significant metal-binding site is comprised of residues from UreG and another urease-related protein.

We identified Cys72 as a nickel ion ligand in UreG$_{Str}$. Replacing this residue with Ala led to a 12-fold increase in the nickel ion K_d, consistent with its participation in the metal-binding site. In addition, titration of nickel ions into UreG$_{Str}$ led to the formation of a 330 nm absorption attributed to a thiolate-to-Ni^{2+} charge-transfer transition which was not generated when Cys72 was absent, implicating this residue as a nickel-coordinating ligand. The corresponding Cys68 residue in *B. pasteurii* UreG also was proposed as a metal ion-binding residue; however, the same residue was identified as forming a disulfide bond that stabilized the dimeric form of that protein (*20*, *23*). Simultaneous function as a disulfide and as a metal ion ligand is unlikely. The corresponding Cys66 residue in *H. pylori* UreG was proposed to be involved in zinc ion binding on the basis of a 10-fold decreased affinity in the C66A variant (*22*), but curiously the effects of this mutation on nickel ion binding were not examined. Our studies of *K. aerogenes* UreG confirm that this conserved cysteine is involved in nickel ion binding and show it does not form an essential disulfide bond.

Other residues comprising the metal ion-binding site of *K. aerogenes* UreG$_{Str}$ were not identified with certainty by our mutagenesis and equilibrium dialysis studies, but some inferences are possible. The E25A and D80A variants exhibited 4-fold increases in nickel ion K_d, and other substitutions had even smaller effects, consistent with nearby residues compensating for the loss of some ligands. Nevertheless, it is notable that mutants expressing the K20A, D49A, C72A, H74A, D80A, and S111A UreG$_{Str}$ proteins in the context of the complete urease gene

cluster were essentially inactive. Lys20 is in the P-loop and Asp49 corresponds to the Mg^{2+} coordinating residue of HypB, thus likely accounting for their essential roles. Based on homology to the HypB structure, we propose that His74 and Ser111 are located close to Cys72 and the former residue is likely to participate in metal binding (while we cannot eliminate the possibility, Ser is much less likely to serve as a metal ligand). The residue corresponding to His74 was mutated in *H. pylori* UreG, and the resulting H68A protein bound zinc ions with lower affinity by an order of magnitude (*22*), again without analysis of the effects on nickel ion binding. For *B. pasteurii* UreG, the metal-binding ligands were proposed to be Glu64, Cys68, and His70, corresponding to Glu68, Cys72, and His74 of the *K. aerogenes* protein (*20*). The lack of effect on urease activity for cells containing E68A $UreG_{Str}$ effectively rules out this Glu residue as an essential metal-binding residue.

The only other cysteine in *K. aerogenes* $UreG_{Str}$, Cys28, is not essential for urease activation, but the urease activity decreased to 13% of nonmutant samples in cells containing the C28A variant. Titration of nickel ions into the C28A variant generated a perturbed UV spectrum, with nearly a 2-fold increase in intensity and a shift of about 30 nm in the absorption feature, indicating a slightly different metal coordinating environment. This change may be associated with the protein's ability to form a dimer in the presence of nickel ions.

In addition to the above new results obtained with purified $UreG_{Str}$, we investigated the interaction of this protein with other urease-related proteins. Soluble extracts of cells expressing the urease gene cluster with *ureG* modified to encode $UreG_{Str}$ were analyzed by pull-down assays. The *Strep*-tagged version of UreG formed a complex that included all other urease components, with the amount of bound UreE enhanced by the presence of nickel ions. A similar UreABC−UreDFG−UreE complex was previously described for a sample in which a hinge-like region of UreB was mutated, resulting in the trapping of this complex (*46*). Those studies led to a model in which the accessory proteins function, in part, to shift the position of the main domain of UreB to allow nickel ions and bicarbonate to gain access to the nascent active site.

When cells expressing the $UreG_{Str}$ variants were examined in the context of the other urease components, Asp80 was identified as being essential for stabilizing the binding of UreG to the UreABC−UreDF complex. Significantly, the D80A variant failed to generate the UreABC−UreDFG−UreE complex; instead, it only interacted with UreE. Asp80 is likely to be positioned at the interface between UreG and the UreABC−UreDF complex. On the basis of prior studies examining urease-related complexes formed with the *K. aerogenes* proteins, UreG most likely binds to UreF (*12*−*14*, *16*). The D80A $UreG_{Str}$−UreE complex indicates that UreE binds to UreG within the UreABC−UreDFG−UreE complex. An interaction between UreG and UreE was previously suggested by two-hybrid analyses of the *H. pylori* proteins (*31*) and by direct biochemical analysis of these proteins from the same microorganism (*24*).

Further investigation of the interaction between $UreG_{Str}$ and UreE used purified proteins and *in vitro* pull-down assays to reveal stabilization of the complex by either nickel or zinc ions. Zinc ion-dependent stabilization of a complex between these proteins was seen previously with the *H. pylori* proteins (*24*), but in that case nickel ions were ineffective for generating the complex. Moreover, the protein stoichiometries of the two complexes differed. Whereas the *H. pylori* proteins formed a zinc-stabilized $(UreG)_2(UreE)_2$ complex, with a dimeric UreG binding to the dimeric UreE, the *K. aerogenes* proteins formed a nickel- or zinc-stabilized complex with one UreE dimer per $UreG_{Str}$ protomer, aggregated into a $[UreG_{Str}(UreE)_2]_3$ complex of ~168 kDa. The Ni-stabilized interaction between *K. aerogenes* $UreG_{Str}$ and UreE, coupled with the Ni-binding capabilities of UreG and UreD (*16*), supports a model in which UreE delivers nickel ions to UreG within the UreABC−UreDFG complex, with the metal ion subsequently passed from UreG to UreD and then into the nascent active site of urease. One or more of the sequential metal ion transfer steps is likely driven by GTP hydrolysis, and the overall process, but not the individual proteins, is specific for nickel ions.

In conclusion, this work describes a new approach to purify *K. aerogenes* UreG using a *Strep* tag, provides critical new insights into the interactions between this protein and nickel and zinc ions, identifies Cys72 as a nickel ligand, demonstrates the necessity of Asp80 for stabilizing UreG binding to UreABC−UreDF, establishes UreG as the site of binding for UreE, and supports a model for sequential metal ion transfer from UreE to UreG to UreD to the urease active site.

ACKNOWLEDGMENT

We thank Brittnie DeVries, Scott Mulrooney, Eric Carter, and Rachel Morr for assistance.

SUPPORTING INFORMATION AVAILABLE

Tables enumerating the plasmids and strains used in these studies and the oligonucleotides employed for mutagenesis. This material is available free of charge via the Internet at http://pubs.acs.org.

REFERENCES

1. Carter, E. L., Flugga, N., Boer, J. L., Mulrooney, S. M., and Hausinger, R. P. (2009) Interplay of metal ions and urease. *Metallomics 1*, 207–221.
2. Krajewska, B. (2009) Ureases I. Functional, catalytic and kinetic properties: A review. *J. Mol. Catal. B: Enzym. 59*, 9–21.
3. Jabri, E., Carr, M. B., Hausinger, R. P., and Karplus, P. A. (1995) The crystal structure of urease from *Klebsiella aerogenes*. *Science 268*, 998–1004.
4. Benini, S., Rypniewski, W. R., Wilson, K. S., Miletti, S., Ciurli, S., and Mangani, S. (1999) A new proposal for urease mechanism based on the crystal structures of the native and inhibited enzyme from *Bacillus pasteurii*: Why urea hydrolysis costs two nickels. *Structure 7*, 205–216.
5. Ha, N. C., Oh, S. T., Sung, J. Y., Cha, K. A., Lee, M. H., and Oh, B. H. (2001) Supramolecular assembly and acid resistance of *Helicobacter pylori* urease. *Nat. Struct. Biol. 8*, 505–509.
6. Sheridan, L., Wilmot, C. M., Cromie, K. D., van der Logt, P., and Phillips, S. E. V. (2002) Crystallization and preliminary X-ray structure determination of jack bean urease with a bound antibody fragment. *Acta Crystallogr., Sect. D: Biol. Crystallogr. 58*, 374–376.
7. Kim, J. K., Mulrooney, S. B., and Hausinger, R. P. (2005) Biosynthesis of active *Bacillus subtilis* urease in the absence of known urease accessory proteins. *J. Bacteriol. 187*, 7150–7154.
8. Quiroz, S., Kim, J. K., Mulrooney, S. B., and Hausinger, R. P. (2007) Chaperones of nickel metabolism, in Nickel and Its Surprising Impact on Nature (Sigel, A., Sidel, H., and Sigel, R. K. O., Eds.) pp 519−544, John Wiley & Sons, Chichester, U.K.
9. Lee, M. H., Mulrooney, S. B., and Hausinger, R. P. (1990) Purification, characterization, and *in vivo* reconstitution of *Klebsiella aerogenes* urease apoenzyme. *J. Bacteriol. 172*, 4427–4431.
10. Jabri, E., and Karplus, P. A. (1996) Structures of the *Klebsiella aerogenes* urease apoenzyme and two active-site mutants. *Biochemistry 35*, 10616–10626.
11. Park, I. S., Carr, M. B., and Hausinger, R. P. (1994) In vitro activation of urease apoprotein and role of UreD as a chaperone required for

nickel metallocenter assembly. *Proc. Natl. Acad. Sci. U.S.A. 91*, 3233–3237.
12. Moncrief, M. B. C., and Hausinger, R. P. (1996) Purification and activation properties of UreD-UreF-urease apoprotein complexes. *J. Bacteriol. 178*, 5417–5421.
13. Moncrief, M. B. C., and Hausinger, R. P. (1997) Characterization of UreG, identification of a UreD-UreF-UreG complex, and evidence suggesting that a nucleotide-binding site in UreG is required for in vivo metallocenter assembly of *Klebsiella aerogenes* urease. *J. Bacteriol. 179*, 4081–4086.
14. Soriano, A., and Hausinger, R. P. (1999) GTP-dependent activation of urease apoprotein in complex with the UreD, UreF, and UreG accessory proteins. *Proc. Natl. Acad. Sci. U.S.A. 96*, 11140–11144.
15. Soriano, A., Colpas, G. J., and Hausinger, R. P. (2000) UreE stimulation of GTP-dependent urease activation in the UreD-UreF-UreG-urease apoprotein complex. *Biochemistry 39*, 12435–12440.
16. Carter, E. L., and Hausinger, R. P. (2010) Characterization of *Klebsiella aerogenes* urease accessory protein UreD in fusion with the maltose binding protein. *J. Bacteriol. 192*, 2294–2304.
17. Kim, J. K., Mulrooney, S. B., and Hausinger, R. P. (2006) The UreEF fusion protein provides a soluble and functional form of the UreF urease accessory protein. *J. Bacteriol. 188*, 8413–8420.
18. Kim, K. Y., Yang, C. H., and Lee, M. H. (1999) Expression of the recombinant *Klebsiella aerogenes* UreF protein as a MalE fusion. *Arch. Pharm. Res. 22*, 274–278.
19. Salomone-Stagni, M., Zambelli, B., Musiani, F, and Ciurli, S. (2007) A model-based proposal for the role of UreF as a GTPase-activating protein in the urease active site biosynthesis. *Proteins 68*, 749–761.
20. Zambelli, B., Stola, M., Musiani, F., De Vriendt, K., Samyn, B., Devreese, B., Van Beeumen, J., Turano, P., Dikiy, A., Bryant, D. A., and Ciurli, S. (2005) UreG, a chaperone in the urease assembly process, is an intrinsically unstructured GTPase that specifically binds Zn^{2+}. *J. Biol. Chem. 280*, 4684–4695.
21. Zambelli, B., Musiani, F., Savini, M., Tucker, P., and Ciurli, S. (2007) Biochemical studies on *Mycobacterium tuberculosis* UreG and comparative modeling reveal structural and functional conservation among the bacterial UreG family. *Biochemistry 46*, 3171–3182.
22. Zambelli, B., Turano, P., Musiani, F., Neyroz, P., and Ciurli, S. (2009) Zn^{2+} linked dimerization of UreG from *Helicobacter pylori*, a chaperone involved in nickel trafficking and urease activation. *Proteins 74*, 222–239.
23. Neyroz, P., Zambelli, B., and Ciurli, S. (2006) Intrinsically disordered structure of *Bacillus pasteurii* UreG as revealed by steady-state and time-resolved fluorescence spectroscopy. *Biochemistry 45*, 8918–8930.
24. Bellucci, M., Zambelli, B., Musiani, F., Turano, P., and Ciurli, S. (2009) *Helicobacter pylori* UreE, a urease accessory protein: specific Ni^{2+}- and Zn^{2+}-binding properties and interaction with its cognate UreG. *Biochem. J. 422*, 91–100.
25. Gasper, R., Scrima, A., and Wittinghofer, A. (2006) Structural insights into HypB, a GTP-binding protein that regulates metal binding. *J. Biol. Chem. 281*, 27492–27502.
26. Leach, M. R., and Zamble, D. B. (2007) Metallocenter assembly of the hydrogenase enzymes. *Curr. Opin. Chem. Biol. 11*, 159–165.
27. Colpas, G. J., Brayman, T. G., Ming, L. J., and Hausinger, R. P. (1999) Identification of metal-binding residues in the *Klebsiella aerogenes* urease nickel metallochaperone, UreE. *Biochemistry 38*, 4078–4088.
28. Musiani, F., Zambelli, B., Stola, M., and Ciurli, S. (2004) Nickel trafficking: Insights into the fold and function of UreE, a urease metallochaperone. *J. Inorg. Biochem. 98*, 803–813.
29. Song, H. K., Mulrooney, S. B., Huber, R., and Hausinger, R. P. (2001) Crystal structure of *Klebsiella aerogenes* UreE, a nickel-binding metallochaperone for urease activation. *J. Biol. Chem. 276*, 49359–49364.
30. Remaut, H., Safarov, N., Ciurli, S., and Van Beeumen, J. (2001) Structural basis for Ni^{2+} transport and assembly of the urease active site by the metallochaperone UreE from *Bacillus pasteurii*. *J. Biol. Chem. 276*, 49365–49370.
31. Rain, J. C., Selig, L., De Reuse, H., Battaglia, V., Reverdy, C., Simon, S., Lenzen, G., Petel, F., Wojcik, J., Schachter, V., Chemama, Y., Labigne, A. S., and Legrain, P. (2001) The protein-protein interaction map of *Helicobacter pylori*. *Nature 409*, 211–215.
32. Laemmli, U. K. (1970) Cleavage of structural proteins during assembly of head of bacteriophage-T4. *Nature 227*, 680.
33. Lee, M. H., Pankratz, H. S., Wang, S., Scott, R. A., Finnegan, M. G., Johnson, M. K., Ippolito, J. A., Christianson, D. W., and Hausinger, R. P. (1993) Purification and characterization of *Klebsiella aerogenes* UreE protein: A nickel-binding protein that functions in urease metallocenter assembly. *Protein Sci. 2*, 1042–1052.
34. Whitmore, L., and Wallace, B. A. (2004) DICHROWEB, an online server for protein secondary structure analyses from circular dichroism spectroscopic data. *Nucleic Acids Res. 32*, W668–W673.
35. Weatherburn, M. W. (1967) Phenol-hypochlorite reaction for determination of ammonia. *Anal. Chem. 39*, 971–974.
36. Hunt, J. B., Neece, S. H., and Ginsburg, A. (1985) The use of 4-(2-pyridylazo) resorcinol in studies of zinc release from *Escherichia coli* aspartate transcarbamoylase. *Anal. Biochem. 146*, 150–157.
37. Mulrooney, S. B., Pankratz, H. S., and Hausinger, R. P. (1989) Regulation of gene-expression and cellular-localization of cloned *Klebsiella aerogenes* (*Klebsiella pneumoniae*) urease. *J. Gen. Microbiol. 135*, 1769–1776.
38. Skerra, A., and Schmidt, T. G. M. (2000) Use of the Strep-tag and streptavidin for detection and purification of recombinant proteins, in Applications of Chimeric Genes and Hybrid Proteins, Part A, pp 271−304, Academic Press, San Diego.
39. Maier, T., Drapal, N., Thanbichler, M., and Böck, A. (1998) Strep-tag II affinity purification: An approach to study intermediates of metalloenzyme biosynthesis. *Anal. Biochem. 259*, 68–73.
40. Larkin, M. A., Blackshields, G., Brown, N. P., Chenna, R., McGettigan, P. A., McWilliam, H., Valentin, F., Wallace, I. M., Wilm, A., Lopez, R., Thompson, J. D., Gibson, T. J., and Higgins, D. G. (2007) Clustal W and clustal X version 2.0. *Bioinformatics 23*, 2947–2948.
41. Leipe, D. D., Wolf, Y. I., Koonin, E. V., and Aravind, L. (2002) Classification and evolution of P-loop GTPases and related ATPases. *J. Mol. Biol. 317*, 41–72.
42. Kozlowski, H., Révérend, B. D.-L., Ficheux, D., Loucheux, C., and Sovago, I. (1987) Nickel(II) complexes with sulfhydryl containing peptides. Potentiometric and spectroscopic studies. *J. Inorg. Biochem. 29*, 187–197.
43. Hubbard, P. A., Padovani, D., Labunska, T., Mahlstedt, S. A., Banerjee, R., and Drennan, C. L. (2007) Crystal structure and mutagenesis of the metallochaperone MeaB: Insight into the causes of methylmalonic aciduria. *J. Biol. Chem. 282*, 31308–31316.
44. Khil, P. P., Obmolova, G., Teplyakov, A., Howard, A. J., Gilliland, G. L., and Camerini-Otero, R. D. (2004) Crystal structure of the *Escherichia coli* YjiA protein suggests a GTP-dependent regulatory function. *Proteins 54*, 371–374.
45. Padovani, D., and Banerjee, R. (2009) A G-protein editor gates coenzyme B-12 loading and is corrupted in methylmalonic aciduria. *Proc. Natl. Acad. Sci. U.S.A. 106*, 21567–21572.
46. Quiroz-Valenzuela, S., Sukuru, S. C. K., Hausinger, R. P., Kuhn, L. A., and Heller, W. T. (2008) The structure of urease activation complexes examined by flexibility analysis, mutagenesis, and small-angle X-ray scattering. *Arch. Biochem. Biophys. 480*, 51–57.